

A variational framework for fiber-reinforced viscoelastic soft tissues

J. M. Vassoler^{*,†}, L. Reips and E. A. Fancello

Department of Mechanical Engineering, Federal University of Santa Catarina, Florianópolis, SC, Brazil

SUMMARY

The mechanical properties of soft biological tissues vary depending on how the internal structure is organized. Classical examples of tissues are ligaments, tendons, skin, arteries, and annulus fibrous. The main element of such tissues is the fibers which are responsible for the tissue resistance and the main mechanical characteristic is their viscoelastic anisotropic behavior. The objective of this paper is to extend an existing model for isotropic viscoelastic materials in order to include anisotropy provided by fiber reinforcement. The incorporation of the fiber allows the mechanical behavior of these tissues to be simulated. The model is based on a variational framework in which its mechanical behavior is described by a free energy incremental potential whose local minimization provides the constraints for the internal variable updates for each load increment. The main advantage of this variational approach is the ability to represent different material models depending on the choice of suitable potential functions. Finally, the model is implemented in a finite-element code in order to perform numerical tests to show the ability of the proposed model to represent fiber-reinforced materials. The material parameters used in the tests were obtained through parameter identification using experimental data available in the literature. Copyright © 2011 John Wiley & Sons, Ltd.

Received 28 October 2010; Revised 14 July 2011; Accepted 16 August 2011

KEY WORDS: biomechanics; anisotropy; nonlinear viscoelasticity

1. INTRODUCTION

Soft biological tissues, such as skin, ligaments and tendons, are very important for the mechanical functioning of the body. They are responsible, respectively, for the protection of the body, and the transfer of loads between bones and between muscles and bones [1].

Soft biological tissues are formed mainly of elastin and collagen. Elastin, like rubber, is comprised of long flexible molecules that form three-dimensional networks by cross-linking and is responsible for the elasticity of the tissues. Collagen is the most important structural element of soft and hard tissues in animals. The particular arrangement of the collagen proteins - three left-handed helices twisted together into a right-handed triple helix - provides this structure with a high stretch resistance to traction [2]. These molecules can be aggregated to form different structures depending on the tissue. Firstly, the collagen molecules can wrap around themselves to form a collagen fibril which varies according to the animal species and tissue. Subsequently, bundles of collagen fibrils can be organized into collagen fibers and the fibers into tissues, where the packaging of collagen fibers has many different modes of organization that vary depending on the tissue.

Connective tissues, such as ligaments and tendons, have a pronounced anisotropic mechanical behavior due to their internal structure, consisting of regular parallel collagen fibers, which it is the simplest tissue structure. The fiber structure of tendons has a largely parallel organization, and

^{*}Correspondence to: J. M. Vassoler, Department of Mechanical Engineering, Federal University of Rio Grande do Sul, Rua Sarmiento Leite, 425 - Cidade Baixa, 90050-170, Porto Alegre, RS, Brazil.

[†]E-mail: vassoler@mecanica.ufrgs.br

under the relaxed condition it can appear wavy but it becomes straight under tension. Ligaments have a less regular structure than tendons, with the collagen fibers sometimes being curved. They may be stressed differently for different functions of the ligament. The three-dimensional networks of collagen in the skin are more complex, where the predominant fiber direction is parallel to the surface. Due to its complex internal structure the skin allows large strains without stretching of the individual fibers [2].

The mechanical properties of biological tissues vary depending on how the fibers, cells and ground substance are organized. The main features of soft tissues are [2]: nonlinear stress-strain relationship, hysteresis in cyclic loading and unloading, stress relaxation at constant strain, preconditioning in repeated cycles, and also high stretching (15%) without damage [1].

Within the set of interrelated characteristics of soft tissues, the anisotropy induced by fiber reinforcement, the Mullins effect, related to damage and viscoelastic behavior, should also be mentioned.

In relation to the incorporation of a finite viscoelastic representation in soft tissues an isotropic model based on the invariants of the Cauchy and its time derivative has previously been presented [3]. In [4] a viscoelastic model is proposed in which the anisotropy of the fibers is included by means of a structural tensor related to the fiber directions.

Some references using classical models with anisotropy concepts to simulate these materials may be cited. In [5] a nonlinear transversally isotropic law incorporating anisotropy and viscoelasticity is proposed in order to simulate soft connective tissues at finite strain. The constitutive model was used later in [6] where the isotropic and anisotropic contributions were decoupled to model a human anterior cruciate ligament (ACL) under multiaxial loading. The ACL potential was split into the sum of the strain energy functions representing the response of the ground substance and the anisotropic behavior introduced by the collagen fibers. In [7] is proposed a thermodynamically consistent model to describe softening phenomena in anisotropic materials. The model was able to reproduce the general characteristics of preconditioning including hysteresis, stabilization of the response and residual deformations.

In [8] an experimental study on the preconditioned response of porcine dermal tissue to stretch and load-controlled cyclic deformation is presented. Samples were preconditioned at each loading rate until the resulting hysteresis loop did not change. Full recovery of the samples to their preloaded condition was then allowed prior to starting a new test. The results show clearly a nonlinear viscoelasticity contribution with no residual deformation reported. In [9] the response of pig skin to different strain rates was investigated. The author states that the mechanical response of the pig skin shows a great strain rate sensitivity indicating the existence of viscoelastic effects. On the other hand [10] presents a uniaxial experimental study of mouse skin behavior for monotonic and cyclic loading where mouse samples were submitted to only one strain rate in order to identify aspects related to the Mullins effect and internal damage. The author reported pronounced internal damage at a high level of cyclic stretching and significant viscoelastic effects due to the fact that the unloading and reloading path do not coincide in the cycle test.

A lack of information on the relationship between the mechanical properties of the fibers and the isotropic matrix was observed in the literature. In [11] the author reports experimental results which indicate the existence of three regions on a typical stress-strain curve for skin. Initially, there is a high degree of deformation at low stress, followed by an intermediate region, and finally, a rapid increase in stress for a small increase in strain until failure. The author attributes the mechanical response at low level of stress to the soft part of the dermis, where there is a random network of collagen fibers. Thus, as the fibers straighten they do not carry load until some of them become completely straight (start of the intermediate region). As the deformation progresses, additional fibers take part in the load-carrying process until all fibers are involved. At this point the behavior is controlled by the stiff collagen fibers. Moreover, the author states that the mechanical behavior in the first region is elastic and almost linear, where it can be considered to have a Young's modulus with a value around 100 times smaller than that of a soft rubber.

A general framework for viscoelastic materials proposed in [12] shows features suitable to represent the mechanical behavior of soft biological tissues. This framework is based on the variational mathematical background presented in [13] and [14], which was also used to model porous plasticity

in [15] and non-cohesive granular media in [16] among many other inelastic phenomena. The constitutive formulation of [12] for non-linear finite viscoelastic materials is distinct from [13] in terms of the possibility to accommodate a wide set of models depending on the choice of potentials, allowing its use for many viscoelastic materials. In [17–19] the variational approach was applied to characterize and simulate soft tissue. In [20], a viscoplastic contribution has incorporated into the non-linear viscoelastic model [12]. This constitutive model is able to represent important inelastic behaviors present in soft tissues: non-linear stress-strain relationship, irreversible, dissipative and rate-dependent behavior. However, it cannot reproduce the anisotropy found in the connective tissues or internal damage.

Since the constitutive behavior of skin is predominantly represented by the collagen fibers, the fiber contribution should take into account the viscous effects noted in [8–10], besides the clear anisotropy. Thus, the objective of this work is to extend the isotropic viscoelastic variational framework presented in [12] to include fiber-reinforced viscoelastic behaviors in order to provide viscoelastic anisotropy. The new framework allows the simulation of the anisotropy of biological tissue with viscoelasticity without considering internal damage.

In Section 2 the mathematical background of the variational framework is presented. Section 3 applies this approach to the isotropic and fiber-reinforced viscoelastic models. Finally, Section 4 shows examples to evaluate the performance of the proposed model while Section 5 presents the conclusions.

2. VARIATIONAL CONSTITUTIVE MODEL

Hyperelastic models are based on the existence of a free energy function W which is dependent only on the total strain and whose derivative provides the stress state of that material point. The first Piola-Kirchhoff stress tensor \mathbf{P} can be defined as

$$\mathbf{P} = \frac{\partial W(\mathbf{F})}{\partial \mathbf{F}} = 2\mathbf{F} \frac{\partial W(\mathbf{C})}{\partial \mathbf{C}} \tag{1}$$

where \mathbf{F} is the gradient of deformation and $\mathbf{C} = \mathbf{F}^T \mathbf{F}$ the Cauchy-Green tensor.

Considering that the compatibility and constitutive equations are satisfied, and \mathcal{K} is the set of admissible configurations, the equilibrium problem is related to the minimization of potential $\mathcal{H}(x)$, as follows:

$$\min_{x \in \mathcal{K}} \mathcal{H}(x) \tag{2}$$

$$\mathcal{H}(x) = \int_{\Omega_0} W(\mathbf{C}(x)) d\Omega_0 - \left[\int_{\Omega_0} \mathbf{b}_0 \cdot x d\Omega_0 + \int_{\Gamma_0} f_0 \cdot x d\Gamma_0 \right] \tag{3}$$

The constitutive expression given in Equation (1) does not apply to dissipative materials since the stress state is dependent not only on the total strain but also on the strain history. Despite this difficulty, an approach is proposed in [13] in which the constitutive problem can be stated analogously to Equation (1) in an incremental way. In this approach a pseudo-potential energy, also called the incremental potential, is defined at each load step, providing the first Piola-Kirchhoff stress as follows:

$$\mathbf{P}_{n+1} = \frac{\partial \Psi(\mathbf{F}_{n+1}; \xi_n)}{\partial \mathbf{F}_{n+1}} = 2\mathbf{F}_{n+1} \frac{\partial \Psi(\mathbf{C}_{n+1}; \xi_n)}{\partial \mathbf{C}_{n+1}} \tag{4}$$

In this expression, $\xi = \{\mathbf{F}, \mathbf{F}^i, \mathbf{Q}\}$ is the set of external and internal state variables. The elastic and inelastic gradients of deformation \mathbf{F}^e and \mathbf{F}^i are obtained from the multiplicative decomposition of \mathbf{F} . The symbol \mathbf{Q} includes all remaining internal variables related to the dissipative phenomena. In [13] it is shown that the incremental potential may have the expression:

$$\Psi(\mathbf{F}_{n+1}; \xi_n) = \min_{\mathbf{F}_{n+1}^i, \mathbf{Q}_{n+1}} \left\{ W(\xi_{n+1}) - W(\xi_n) + \Delta t \psi \left(\mathring{\mathbf{F}}^i, \mathring{\mathbf{Q}}; \xi_n \right) \right\} \tag{5}$$

$$W(\xi) = \varphi(\mathbf{F}) + \varphi^e(\mathbf{F}\mathbf{F}^{i-1}) + \varphi^i(\mathbf{F}^i, \mathbf{Q}) \tag{6}$$

The strain energy allows an additive decomposition into contributions φ , φ^e and φ^i , depending on the total value of \mathbf{F} , on the elastic part \mathbf{F}^e and on the inelastic part \mathbf{F}^i and internal variables \mathbf{Q} respectively. ψ is the (pseudo) potential that provides the dependence of the stress on the rate (incremental approximation of rate) variables $\dot{\mathbf{F}}^i$ and $\dot{\mathbf{Q}}$.

In Equation (5), the minimization problem identifies the optimal values of \mathbf{F}_{n+1}^i and \mathbf{Q}_{n+1} , which define the internal variables associated with the new state \mathbf{F}_{n+1} . Once this minimization problem is solved, stresses may be computed by Equation (4) as in hyperelastic models. Different material models may be constructed in this general framework depending on the particular choices and arrangements of potentials φ , φ^e , φ^i and ψ .

3. FIBER-REINFORCED VISCOELASTIC MODEL

The anisotropic viscoelastic model here proposed is based on an additive decomposition of the incremental potential into an isotropic and a fiber-reinforcement contribution:

$$\Psi = \Psi_{iso} + \Psi_f \tag{7}$$

The potential Ψ_{iso} corresponds to the formulation proposed in [12] for isotropic viscoelastic materials, while Ψ_f is a potential that incorporates the fiber behavior. Figure 1 shows a rheological representation of the addition (7) in which both the isotropic and the fiber contributions are connected in parallel, reacting independently of each other for the same total strain. So, is important to remark at this point the way in which the fiber reinforcement is treated in this proposed model. The additive decomposition in Equation (7) clearly states that the incremental potential of the isotropic matrix and that of the fibers are uncoupled. Both of them depend on the given strain increment over Δt and the constitutive response of the composite comes only from the additive constitutive response of each component. Again, this is clearly illustrated in Figure 1, where each branch of the model represents an additive contribution on the total potential in a continuum macromechanical approach. Moreover, this model considers that fibers are continuously distributed in the isotropic ground substance (matrix) [21] and therefore, no distinction is made on the size or length of them.

3.1. Isotropic incremental potential

As mentioned above, the incremental potential Ψ_{iso} is exactly that presented in [12]. Nevertheless, we use this section to make a brief description of this model in order to keep the text minimally self-contained. We begin by assuming a classical multiplicative decomposition of the gradient of deformation into isochoric and volumetric parts $\mathbf{F} = J\hat{\mathbf{F}}$ with $J = \det(\mathbf{F})$. The isochoric part allows also for a multiplicative separation into elastic and viscous contributions: $\hat{\mathbf{F}}^i = \hat{\mathbf{F}}^e \mathbf{F}^v$. With these

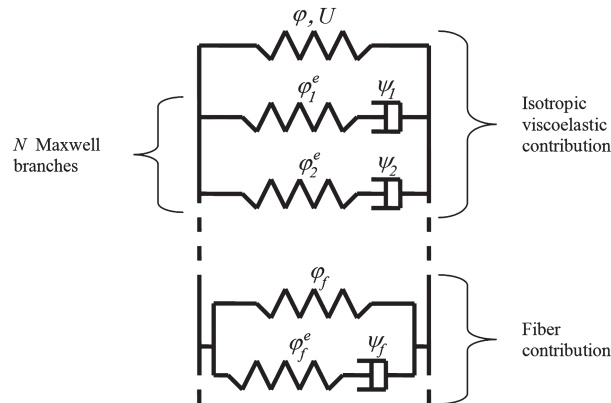


Figure 1. Rheological model.

hypotheses, the free energy[‡] W is defined as

$$W(\mathbf{C}) = U(J) + \varphi(\hat{\mathbf{C}}) + \varphi^e(\hat{\mathbf{C}}^e) \tag{8}$$

where

$$\hat{\mathbf{C}} = \hat{\mathbf{F}}^T \hat{\mathbf{F}} \quad \hat{\mathbf{C}}^e = \hat{\mathbf{F}}^{eT} \hat{\mathbf{F}}^e \tag{9}$$

The isochoric potential φ is an isotropic function of the eigenvalues c_i of \mathbf{C} . The (elastic) volumetric contribution originates from the potential U which is dependent on J :

$$U(J) = \frac{k}{2} [\ln J]^2 \tag{10}$$

The potentials φ, φ^e and ψ are assumed to be isochoric functions of the Cauchy tensors $\hat{\mathbf{C}}, \hat{\mathbf{C}}^e$ and of the viscous stretching \mathbf{D}^v by means of their respective eigenvalues c_i, c_i^e and d_i^v :

$$\varphi(\hat{\mathbf{C}}) = \varphi(c_1, c_2, c_3), \quad \hat{\mathbf{C}} = \sum_{j=1}^3 c_j \mathbf{e}_j \otimes \mathbf{e}_j = \sum_{j=1}^3 c_j \mathbf{E}_j \tag{11}$$

$$\varphi^e(\hat{\mathbf{C}}^e) = \varphi(c_1^e, c_2^e, c_3^e), \quad \hat{\mathbf{C}}^e = \sum_{j=1}^3 c_j^e \mathbf{e}_j^e \otimes \mathbf{e}_j^e = \sum_{j=1}^3 c_j^e \mathbf{E}_j^e \tag{12}$$

$$\psi(\mathbf{D}^v) = \psi(d_1^v, d_2^v, d_3^v), \quad \mathbf{D}^v = \sum_{j=1}^3 d_j^v \mathbf{m}_j^v \otimes \mathbf{m}_j^v = \sum_{j=1}^3 d_j^v \mathbf{M}_j^v \tag{13}$$

where $\mathbf{e}_j, \mathbf{e}_j^e$ and \mathbf{m}_j^v are the eigenvectors and $\mathbf{E}_j, \mathbf{E}_j^e$ and \mathbf{M}_j^v are the eigenprojections of the corresponding tensors. The viscous stretching \mathbf{D}^v is defined by

$$\mathbf{D}^v = \text{Sym}(\mathbf{L}^v) = \mathbf{L}^v = \dot{\mathbf{F}}^v \mathbf{F}^{v-1} \tag{14}$$

where it is defined that \mathbf{L}^v is symmetric. The viscous flow is assumed to be isochoric by means of the following constrains on the spectral components of \mathbf{D}^v

$$\begin{aligned} d_j^v \in K_Q &= \{p_j \in \mathbb{R} \Rightarrow p_1 + p_2 + p_3 = 0\} \\ \mathbf{M}_j^v \in K_M &= \{\mathbf{N}_j \in \text{Sym} \Rightarrow \mathbf{N}_j \cdot \mathbf{N}_j = 1, \mathbf{N}_i \cdot \mathbf{N}_j = 0, i \neq j\} \end{aligned} \tag{15}$$

From these definitions, it is shown in [12] that at each time increment Δt , the isotropic incremental potential in Equation (5), takes the form

$$\Psi_{iso}(\mathbf{F}_{n+1}; \xi_n) = \Delta\varphi(\hat{\mathbf{C}}_{n+1}) + \Delta U(J_{n+1}) + \min_{\mathbf{M}_j^v, \Delta q_j^v} \left\{ \Delta\varphi^e(\hat{\mathbf{C}}_{n+1}^e) + \Delta t \psi(\mathbf{D}_{n+1}^v) \right\} \tag{16}$$

subject to

$$d_j^v = \frac{\Delta q_j^v}{\Delta t}, \quad \Delta q_j^v \in K_Q = \{p_j \in \mathbb{R} \Rightarrow p_1 + p_2 + p_3 = 0\} \tag{17}$$

$$\mathbf{M}_j^v \in K_M = \{\mathbf{N}_j \in \text{Sym} \Rightarrow \mathbf{N}_j \cdot \mathbf{N}_j = 1, \mathbf{N}_i \cdot \mathbf{N}_j = 0, i \neq j\} \tag{18}$$

In expression (16) we have

$$\begin{aligned} \Delta\varphi(\hat{\mathbf{C}}_{n+1}) &= \varphi(\hat{\mathbf{C}}_{n+1}) - \varphi(\hat{\mathbf{C}}_n) \\ \Delta\varphi^e(\hat{\mathbf{C}}_{n+1}^e) &= \varphi^e(\hat{\mathbf{C}}_{n+1}^e) - \varphi^e(\hat{\mathbf{C}}_n^e) \\ \Delta U(J_{n+1}) &= U(J_{n+1}) - U(J_n) \end{aligned} \tag{19}$$

[‡] For simplicity of notation we omit the subscript *iso* from the potentials associated with the isotropic contributions. However, we maintain the subscript *f* for the potentials associated with the fiber counterpart.

with

$$\begin{aligned} \hat{\mathbf{C}}_{n+1}^e &= \hat{\mathbf{F}}_{n+1}^{eT} \hat{\mathbf{F}}_{n+1}^e = \hat{\mathbf{C}}^{pr} (\exp[\Delta t \mathbf{D}_{n+1}^v])^{-2} \\ \hat{\mathbf{C}}^{pr} &= \mathbf{F}_n^{v-T} \hat{\mathbf{C}}_{n+1} \mathbf{F}_n^{v-1} \Delta t \mathbf{D}_{n+1}^v = \sum_{j=1}^3 \Delta q_j^v \mathbf{M}_j \\ \mathbf{F}_{n+1}^v \mathbf{F}_n^{v-1} &= \exp[\Delta t \mathbf{D}_{n+1}^v] \hat{\mathbf{F}}_{n+1}^e = \hat{\mathbf{F}}_{n+1} \hat{\mathbf{F}}_{n+1}^{v-1} \end{aligned} \tag{20}$$

The optimality condition of (16) with respect to \mathbf{M}_j^v results in $\hat{\mathbf{C}}_{n+1}^e$, $\hat{\mathbf{C}}^{pr}$ and \mathbf{D}^v sharing the same eigenvectors $\mathbf{E}_j^e = \mathbf{E}_j^{pr} = \mathbf{M}_j^v$ respectively. Finally, the minimization with respect to Δq_j^v results in the following set of nonlinear equations [12]:

$$\begin{aligned} \frac{\partial \varphi^e}{\partial \varepsilon_j^e} - \frac{\partial \psi}{\partial d_j^v} + \lambda &= 0 \quad j = 1, 2, 3 \\ \Delta q_1^v + \Delta q_2^v + \Delta q_3^v &= 0 \end{aligned} \tag{21}$$

where λ is the Lagrangian multiplier associated with the constraint (17) and $\varepsilon_j^e = \frac{1}{2} \ln(c_j^e)$. The four nonlinear equations (21) can be solved by the Newton method, a technique that also provides the analytical tangent modulus to be used in the global equilibrium problem. Once the minimizers Δq_j^v are obtained, the first Piola-Kirchhoff stress tensor is calculated by the classic ‘‘hyperelastic-like’’ expression

$$\mathbf{P}_{n+1} = 2\mathbf{F}_{n+1} \frac{\partial \Psi(\mathbf{C}_{n+1}; \mathcal{E}_n)}{\partial \mathbf{C}_{n+1}} = \mathbf{F}_{n+1} \left[J_{n+1}^{-2/3} \text{DEV} \left(2 \frac{\partial \varphi^e}{\partial \hat{\mathbf{C}}_{n+1}} \right) + \frac{\partial U}{\partial J_{n+1}} J_{n+1} \mathbf{C}_{n+1}^{-1} \right] \tag{22}$$

with

$$\frac{\partial \varphi^e}{\partial \hat{\mathbf{C}}_{n+1}} = \mathbf{F}_n^{v-1} \left(\sum_{j=1}^3 \frac{\partial \varphi^e}{\partial \varepsilon_j^e} \frac{1}{2c_j^{pr}} \mathbf{M}_j^v \right) \mathbf{F}_n^{v-T}. \tag{23}$$

c_j^{pr} being the eigenvalues of $\hat{\mathbf{C}}^{pr}$. Detailed information regarding these operations is found in [12].

3.2. Fiber incremental potential

We will now focus on the new terms originating from the addition of fibers. Consider an arrangement (family) of fibers all oriented along a direction \mathbf{a}_f defined on the reference configuration. Since they introduce an anisotropic behavior related to their directions, the corresponding incremental potential is not only dependent on the Cauchy tensor \mathbf{C} , but also on the structural tensor $\mathbf{A}_f = \mathbf{a}_f \otimes \mathbf{a}_f$, where \mathbf{a}_f is the unit vector defining the fiber direction. This dependence in the present case is related to the invariant I_f [4]:

$$I_f = \hat{\mathbf{C}} : \mathbf{A}_f = \mathbf{a}_f \cdot \hat{\mathbf{C}} \cdot \mathbf{a}_f = \lambda_f^2 \tag{24}$$

which has the particular physical interpretation of the quadratic stretch in the direction of the fiber. Other invariants related to the cross relationships between different fiber directions may also be set as strain measurements. However, these invariants are frequently avoided in practice due to the difficulties associated with the material parameter identification for such contribution terms. The total elongation λ_f may be decomposed into elastic and viscous contributions: $\lambda_f = \lambda_f^e \lambda_f^v$. The logarithmic strains related to the elongations and viscous stretching are defined in the usual manner:

$$\begin{aligned} \varepsilon_f &= \ln \lambda_f, \quad \varepsilon_f^e = \ln \lambda_f^e, \quad \varepsilon_f^v = \ln \lambda_f^v \\ d_f^v &= \dot{\lambda}_f^v / \lambda_f^v \end{aligned} \tag{25}$$

The incremental evolution of the viscous stretch is obtained using the exponential mapping proposed in [22] that allows us to write

$$\begin{aligned} \lambda_{f_{n+1}}^v &= \exp\left(\Delta t d_f^v\right) \lambda_{f_n}^v, \quad \Delta \varepsilon_f^v = \Delta t d_f^v = \ln\left(\frac{\lambda_{f_{n+1}}^v}{\lambda_{f_n}^v}\right) = \ln\left(\Delta \lambda_f^v\right) \\ \varepsilon_{f_{n+1}}^e &= \varepsilon_{f_{n+1}} - \varepsilon_{f_{n+1}}^v = \varepsilon_{f_{n+1}} - \left(\varepsilon_{f_n}^v + \Delta \varepsilon_f^v\right) = \varepsilon_f^{pr} - \Delta \varepsilon_f^v \end{aligned} \tag{26}$$

The analogy between expressions (20) and (26) thus becomes clear, and the latter can be considered as the one-dimensional counterpart of the former. With these definitions and following the arguments detailed in [12] the fiber incremental potential is defined as

$$\Psi_f = \Delta \varphi_f(\lambda_{f_{n+1}}) + \min_{\Delta \varepsilon_f^v} \left\{ \varphi_f^e\left(\varepsilon_f^e\left(\Delta \varepsilon_f^v\right)\right) + \Delta t \psi_f\left(\frac{\Delta \varepsilon_f^v}{\Delta t}\right) \right\} \tag{27}$$

analogously to (16). Physically, the fibers only contribute to the traction, i.e., to positive stretches. Therefore, potentials φ_f , φ_f^e and ψ_f have some particularities, which leads to some care being required in approaching the minimization problem. This will be discussed in detail in Section 3.4.

3.3. Material models

Different materials may be represented, however, a suitable choice of potential function is φ , φ^e , U and ψ in (16) and φ_f , φ_f^e and ψ_f in (27).

3.3.1. Isotropic material models. In the isotropic incremental potential (16), the basic expressions of important hyperelastic models, like the Neo-Hookean, Mooney-Rivlin, Ogden and Hencky models, can be used for the potential functions φ , φ^e and ψ . The Hencky expressions are of the type

$$\varphi = \mu \sum_{j=1}^3 (\varepsilon_j)^2, \quad \varphi^e = \mu^e \sum_{j=1}^3 (\varepsilon_j^e)^2, \quad \psi = \eta^v \sum_{j=1}^3 (d_j^v)^2$$

while the Ogden expressions are written as

$$\varphi = \sum_{j=1}^3 \sum_{p=1}^N \frac{\mu_p}{\alpha_p} \left([\exp(\varepsilon_j)]^{\alpha_p} - 1 \right), \quad \varphi^e = \sum_{j=1}^3 \sum_{p=1}^N \frac{\mu_p^e}{\alpha_p} \left([\exp(\varepsilon_j^e)]^{\alpha_p} - 1 \right), \tag{28}$$

$$\psi = \sum_{j=1}^3 \sum_{p=1}^N \frac{\eta_p^v}{\alpha_p} \left([\exp(d_j^v)]^{\alpha_p} - 1 \right). \tag{29}$$

Symbols μ , μ^e , η^v , μ_p , μ_p^e , η_p^v , α_p are material parameters to be identified. More details on this issue are found in [12].

3.3.2. Fiber material models. The accumulated energy due to the presence of fibers has the main characteristic of being null for compressive strain in the fiber direction. Different expressions of hyperelastic fiber-materials are found in the literature, and in this paper we use that proposed in [4]:

$$\varphi_f^e = \begin{cases} \frac{k_1}{2k_2} \{ \exp[k_2(I_f - 1)^2] - 1 \} & \text{if } \lambda_f > 0 \\ 0 & \text{if } \lambda_f \leq 0 \end{cases} \tag{30}$$

where $I_f = \lambda_f^2$. Similar behavior is set for the dissipative potential ψ_f , attributing a zero value to a compressive viscous stretching:

$$\psi_f(d_f^v) = \begin{cases} \bar{\psi}_f(d_f^v) & \text{if } d_f^v \geq 0 \\ 0 & \text{if } d_f^v < 0 \end{cases} \tag{31}$$

where $\bar{\psi}_f$ is any of the viscous models previously used in the isotropic contribution.

3.4. Minimization operations

Since the isotropic minimization problem (16) was presented and studied extensively in [12], we focus here on the discussion of the minimization expression (27) that corresponds to the dissipative energy balance of the Maxwell branch of the fiber contribution shown in Figure 1. Graphically, this problem may be analyzed for two different cases, depending on the signal of ε_f^{pr} . Consider as an example the material models and parameters shown in Table I and take $\varepsilon_f^{pr} = 0.05$. For this case the graph of the potentials φ^e and ψ and their sum is shown in Figure 2. Note that due to the strict convexity of φ^e and ψ in this region, there exist only one minimum for $\Delta\varepsilon^v$. On the other hand, if $\varepsilon_f^{pr} = -0.05$, the curves take the form shown in Figure 3. In this case, we have multiple solutions

Table I. Material models and parameters for the Maxwell branch of Figure 1.

Potential	Fiber	
	Model	Parameters
φ^e	Holzapfel	$k_1 = 5 \text{ MPa}$ e $k_2 = 50 \text{ MPa}$
ψ	Hencky	$\eta^v = 100 \text{ MPa}\cdot\text{s}^{-1}$

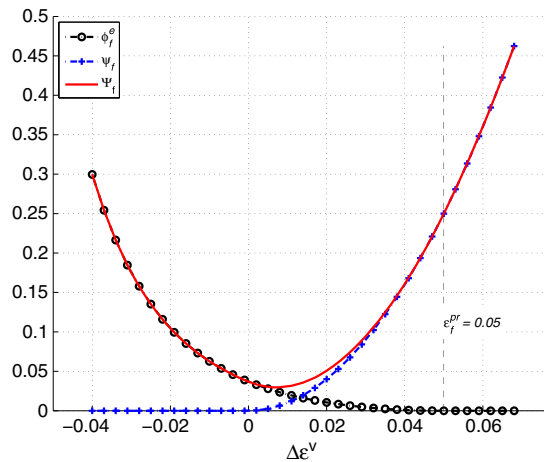


Figure 2. Fiber minimization problem for $\varepsilon_f^{pr} \geq 0$.

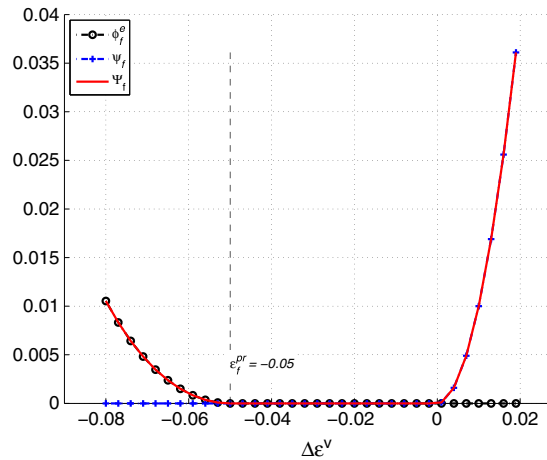


Figure 3. Fiber minimization problem for $\varepsilon_f^{pr} < 0$.

since the arguments $\Delta\varepsilon_f^v$ that solve the minimization belong to the set $[\varepsilon_f^{pr}, 0]$. The choice of different values of $\Delta\varepsilon_f^v$ within the set in these cases leads to different internal variable evolutions and thus to different fiber representations.

In the present case the following strategy is chosen: if $\varepsilon_f^{pr} < 0$ and $\varepsilon_{n+1} \leq 0$, which means that the fiber reaches a shorter configuration than the original one on compression, then $\Delta\varepsilon_f^v$ is set to zero. Conversely, if $\varepsilon_f^{pr} < 0$ and $\varepsilon_{n+1} > 0$ (traction configuration) then $\Delta\varepsilon_f^v = \varepsilon_f^{pr}$.

These assumptions verify that the rheological mechanical behavior is consistent with the observations: the viscous strain ε_f^v cannot reach values greater than the total strain ε_f and the stress contribution provided by the fibers should be null at any instant for a compressive configuration. Figures 4 and 5 show the curves of λ_f^e , λ_f^v and λ_f^{pr} versus time for two different cycles of total stretch λ_f . It is possible to see that λ_f^e , responsible for the stress contribution, is different from zero for positive total stretches.

4. NUMERICAL EXAMPLES

This section presents a set of numerical examples with the aim of showing the ability of the proposed model to simulate the mechanical behavior of fiber reinforced viscoelastic materials. The formulation introduced in this work was implemented in GNU Octave [23] and in the academic finite element code METAFOR [24] - developed by LTAS, Belgium.

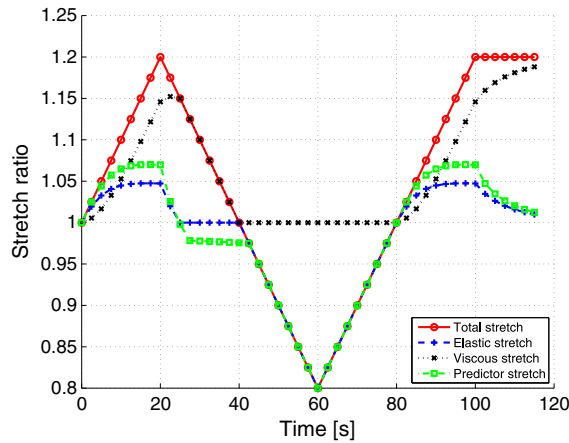


Figure 4. Stretch curves for the first tensile loading.

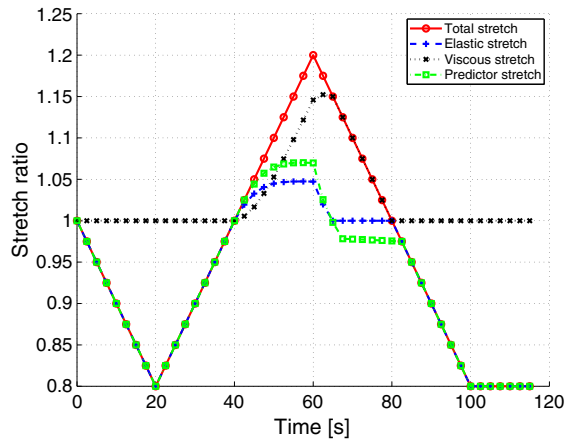


Figure 5. Stretch curves for the first compression loading.

4.1. Parameter identification

Few experimental studies on the mechanical behavior of fiber-reinforced biological tissues are reported in the literature and, frequently, those published have no enough information to characterize the material. Despite this difficulty, a parameter identification based on experimental data is presented in this paper.

The identification was performed using the experimental data presented in [10], where specimens of mouse skin were investigated under cyclic loading at a strain rate of 0.01 s^{-1} . Since no information regarding the orientation of the collagen fibers and transversal strain was provided, the simulations were carried out orientating fibers in the loading direction. The isotropic contribution in the mechanical behavior of skin is known to be much smaller than the fiber contribution. In [11] the author states that the mechanical behavior of human skin may be modeled by an elastic and almost linear model with a Young's modulus value around 100 times smaller than that of a soft rubber. In this study, the isotropic contribution is modeled using the Hencky model with a small constant value $\mu = 2.5 \text{ kPa}$. With this assumption at hand, the identification of the fiber parameters was performed. A merit function based on the square difference between the experimental and numerical data was set and the minimizer point is sought within a feasible box. Table II shows the values obtained through the identification procedure. Figure 6 presents the comparison between the experimental data and numerical curves obtained with the proposed model. From the experimental data in Figure 6 a viscous behavior and a slight loss of load carrying capability of the material can be noted, probably due to internal damage. Besides this damage phenomenon, which is not considered here, the model is able to reproduce the experimental data quite satisfactorily, even for different loading and unloading paths.

4.2. Uniaxial cases

Uniaxial stretching tests are generally the first tests used to visualize the mechanical behavior of proposed constitutive models. Two tests are performed here with controlled stretching cycles as

Table II. Material parameters of the experimental data fitting for the fiber contribution.

Potential	Fiber	
	Model	Parameters
φ	Holzappel	$k_1 = 0.096 \text{ MPa}$ e $k_2 = 8.856 \text{ MPa}$
φ^e	Holzappel	$k_1 = 0.409 \text{ MPa}$ e $k_2 = 20.355 \text{ MPa}$
ψ	Hencky	$\eta^v = 23.526 \text{ MPa}\cdot\text{s}^{-1}$

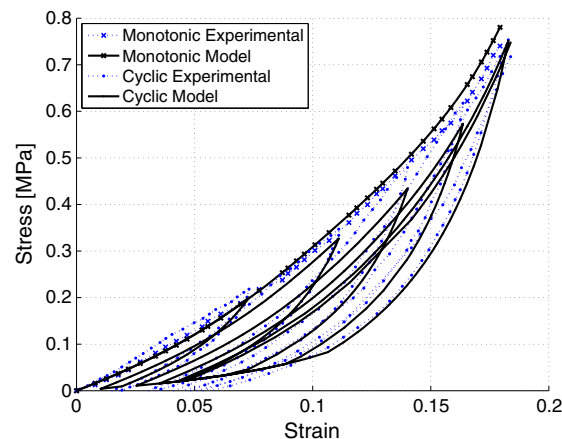


Figure 6. Experimental data fitting for mouse skin.

shown in Figures 4 and 5. The material model is set with the potentials and parameters (Table II) identified in the previous section. The stress/stretch curves obtained are presented in Figures 7 and 8. Both figures show the stiffness of the material for positive strains due to the presence of the fibers. Moreover, the hysteresis shown in the curves is entirely due to the viscous response of the fibers, since the viscous contribution of the isotropic potential is set to zero in these cases.

4.3. Three-dimensional cases

Two cases of solids under finite strain are shown here to illustrate the anisotropic behavior of the proposed model and to emphasize the geometrical nonlinearities. In the first example a membrane-like

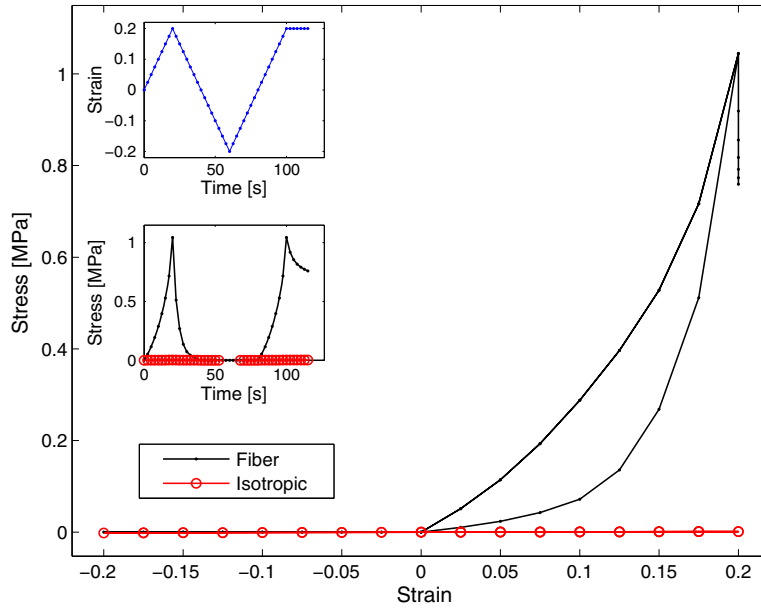


Figure 7. Stress response for the first tensile loading.

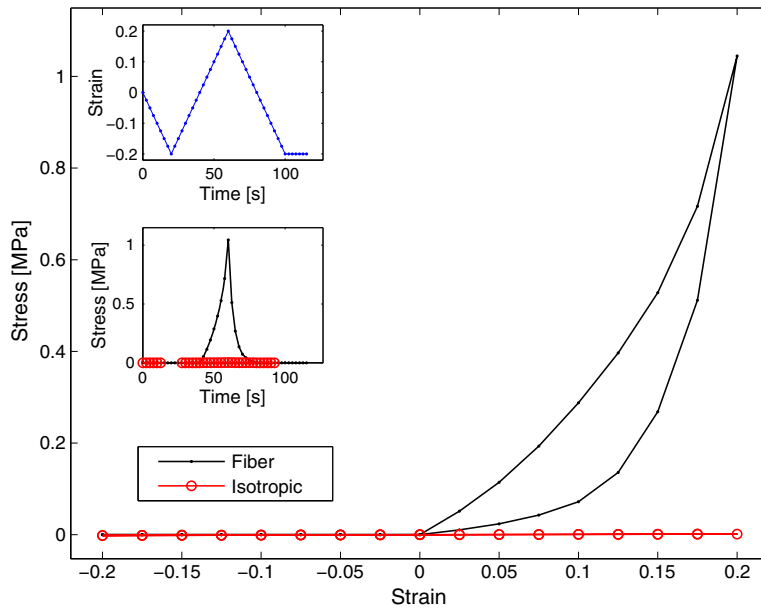


Figure 8. Stress response for the first compressive loading.

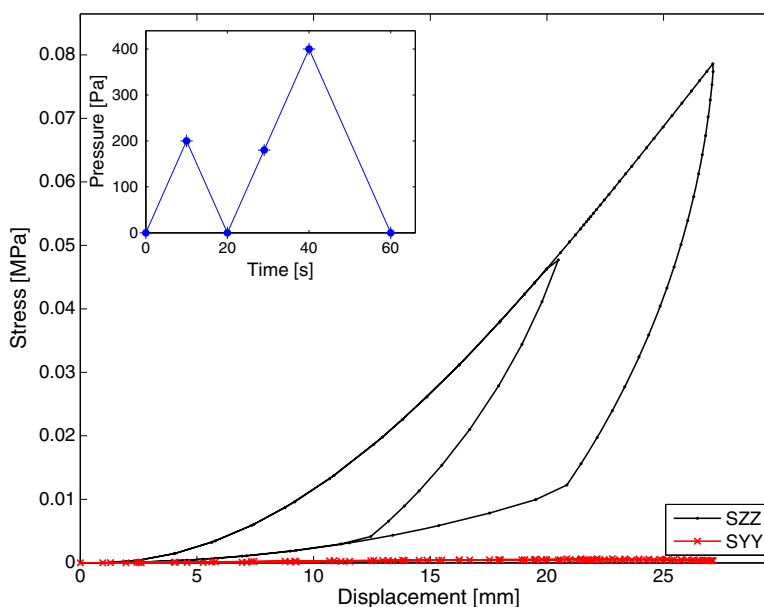


Figure 9. Stress response along the Y and Z directions of the membrane. Cyclic pressure loading.

3D body clamped at its edges is subject to a cyclic pressure loading from below. Figure 9 shows the cyclic pressure applied to the membrane and the stress response along the Y and Z directions.

The material parameters set in Table II are used here, representing a family of fibers oriented along the Z direction. A mesh containing 2400 hexahedral eight-node 3D elements are used to discretize a symmetric quadrant of the membrane. The sequence of deformed configurations at six different time instants is presented in Figure 10, where the anisotropic behavior introduced by the fibers is clearly shown. These configurations correspond to the points highlighted on the curve pressure vs. time presented in Figure 9. The stretching along the Z direction is somewhat contained, while the typical membrane instability rapidly appears for stretches along the Y direction. The problem used an average of 2.87 Newton iterations at each load substep consuming 2.01 seconds each Newton iteration (2.66 GHz microprocessor) with a residual tolerance of $1E - 8$.

A second example shows the anisotropic behavior of a fiber-reinforced composite tube submitted to axial stretching. In this case, the fibers are oriented along a direction of 30° with respect to axial direction. The same material parameters used in the last example are applied in this case. The tube was discretized with 960 hexahedral eight-node 3D elements. The sequence of deformed configurations is shown in Figure 11, where the typical rotation of the reinforced tube can be observed as long as the axial stretching increases, in an attempt to align the fibers in the axial direction. The problem used an average of 2.5 Newton iterations at each load substep consuming 0.79 seconds each Newton iteration (2.66 GHz microprocessor) with a residual tolerance of $1E - 8$.

5. CONCLUSIONS

Despite the difficulties involved in modeling anisotropic tissues, the main objective of this work was achieved. A possible extension of the variational framework for isotropic viscoelastic models to the case of fiber-reinforced materials was developed. The variational framework allows the obtainment of the internal variable updates through the minimization of the respective incremental potentials of the fibers and the isotropic matrix contributions. This minimization is achieved by satisfying the optimality conditions using the Newton iterations. The technical details of the fibers are discussed. Preliminary results show the capability of the proposed anisotropic model to represent fiber-reinforced materials, including rate-dependence of both isotropic and fiber contributions.

A material identification was carried out in order to relate the proposed formulation to a specific material. In particular, parameter identification was performed to characterize an anisotropic

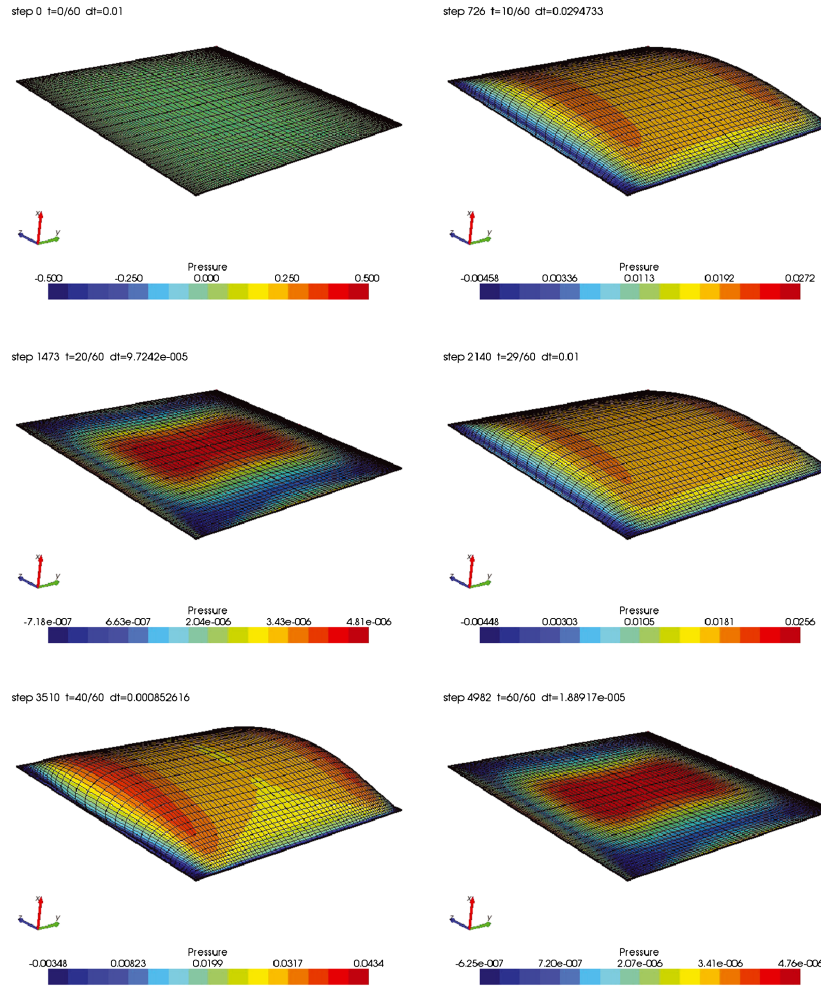


Figure 10. Sequence of configurations of the membrane.

biological tissue. The numerical examples aimed to verify the ability of the proposed approach to follow expected qualitative behaviors. The objective of further studies will be to characterize the mechanical behavior of ligaments and tendons where the anisotropy properties are quite evident.

APPENDIX A: MATERIAL MODELS

A.1. Hencky model

Hencky model is commonly used to model the behavior of vulcanized rubber. The model has a strain energy identical to infinitesimal elasticity.

$$\varphi = \sum_{j=1}^3 \mu (\epsilon_j)^2, \tag{A.1}$$

$$\varphi^e = \sum_{j=1}^3 \mu^e (\epsilon_j^e)^2, \tag{A.2}$$

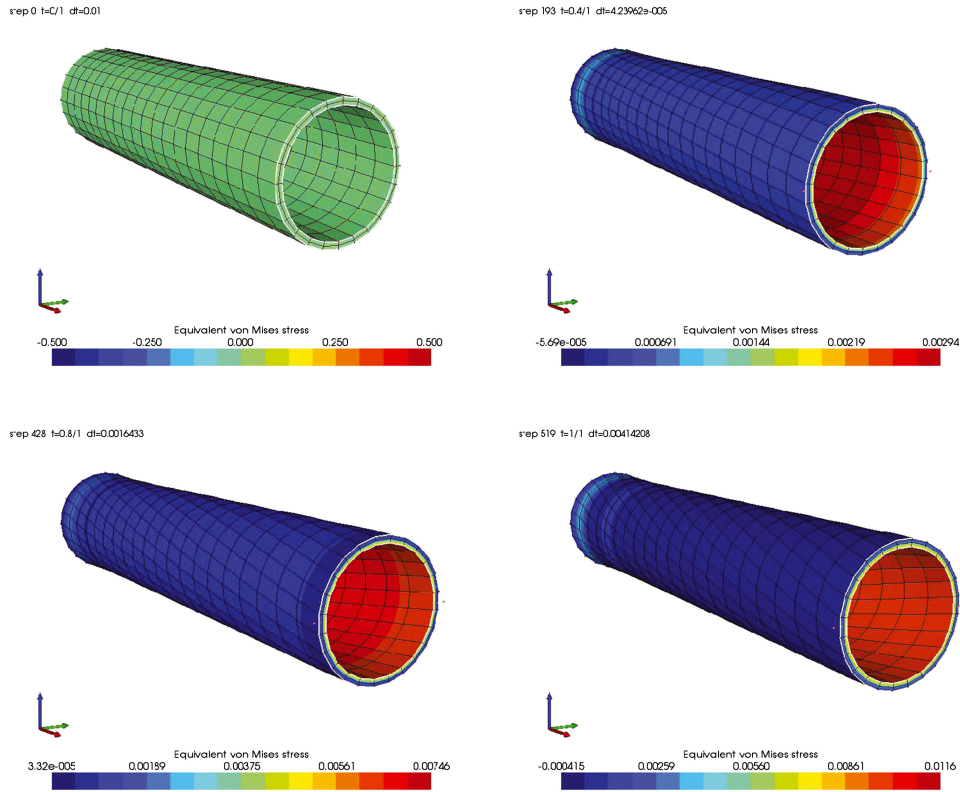


Figure 11. Sequence of configurations of the fiber-reinforced tube.

$$\psi = \sum_{j=1}^3 \eta^v (d_j^v)^2. \tag{A.3}$$

$$\frac{\partial \varphi}{\partial \epsilon_j} = 2\mu \epsilon_j, \tag{A.4}$$

$$\frac{\partial \varphi^e}{\partial \epsilon_j^e} = 2\mu^e \epsilon_j^e, \tag{A.5}$$

$$\frac{\partial \psi}{\partial d_j^v} = 2\eta^v d_j^v. \tag{A.6}$$

A.2. Ogden model

The Ogden model is usually chosen due to its flexibility in representing polymeric materials. For the isotropic contribution the following expressions are used

$$\varphi = \sum_{j=1}^3 \sum_{p=1}^N \frac{\mu_p}{\alpha_p} \left([\exp(\epsilon_j)]^{\alpha_p} - 1 \right), \tag{A.7}$$

$$\varphi^e = \sum_{j=1}^3 \sum_{p=1}^N \frac{\mu_p^e}{\alpha_p} \left([\exp(\epsilon_j^e)]^{\alpha_p} - 1 \right), \tag{A.8}$$

$$\psi = \sum_{j=1}^3 \sum_{p=1}^N \frac{\eta_p^v}{\alpha_p} \left([\exp(d_j^v)]^{\alpha_p} - 1 \right). \tag{A.9}$$

$$\frac{\partial \varphi}{\partial \epsilon_j} = \sum_{p=1}^N \mu_p [\exp(\epsilon_j)]^{\alpha_p}, \tag{A.10}$$

$$\frac{\partial \varphi^e}{\partial \epsilon_j^e} = \sum_{p=1}^N \mu_p^e [\exp(\epsilon_j^e)]^{\alpha_p}, \tag{A.11}$$

$$\frac{\partial \psi}{\partial d_j^v} = \sum_{p=1}^N \eta_p^v [\exp(d_j^v)]^{\alpha_p}, \tag{A.12}$$

A.3. Holzapfel model

In [4] a hyperelastic model is presented in which the collagen fibers are governed by a potential of type

$$\varphi = \frac{k_1}{2k_2} \{ \exp[k_2(I_f - 1)^2] - 1 \} \tag{A.13}$$

$$\varphi^e = \frac{k_1}{2k_2} \left\{ \exp \left[k_2 \left(I_f^e - 1 \right)^2 \right] - 1 \right\} \tag{A.14}$$

where $I_f^e = \left(\lambda_f^e \right)^2$. Note again that these expressions are null, respectively, for $\lambda_f \leq 1$ and $\lambda_f^e \leq 1$.

$$\frac{\partial \varphi}{\partial \lambda_f} = k_1 \left(\exp \left(k_2 \left(\lambda_f^2 - 1 \right)^2 \right) \left(\lambda_f^2 - 1 \right) 2\lambda_f \right); \tag{A.15}$$

$$\frac{\partial \varphi^e}{\partial \lambda_f^e} = k_1 \left(\exp \left(k_2 \left(\left(\lambda_f^e \right)^2 - 1 \right)^2 \right) \left(\left(\lambda_f^e \right)^2 - 1 \right) 2\lambda_f^e \right); \tag{A.16}$$

ACKNOWLEDGEMENTS

Eduardo Alberto Fancello and Jakson Manfredini Vassoler thank the Brazilian "Conselho Nacional de Desenvolvimento Científico e Tecnológico" who provided financial support for this research. We also thank the development team of METAFOR (LTAS-MN²L - Université de Liège, Belgium) for the permission of use and modification of the code.

REFERENCES

1. Pioletti DP, Rakotomanana LR. Non-linear viscoelastic laws for soft biological tissues. *European Journal of Mechanics - A/Solids* 2000; **19**(5):749–759.
2. Fung Y. *Biomechanics: Mechanical Properties of Living Tissues*. Springer: New York, 1993.
3. Pioletti DP, Rakotomanana LR. Viscoelastic constitutive law in large deformations: application to human knee ligaments and tendons. *Journal of Biomechanics* 1998; **31**(8):753–757.
4. Holzapfel G, Gasser TC. A viscoelastic model for fiber-reinforced composites at finite strains: Continuum basis, computational aspects and applications. *Computer Methods in Applied Mechanics and Engineering* 2001; **190**(34):4379–4403.
5. Limbert G, Taylor M. On the constitutive modeling of biological soft connective tissues: A general theoretical framework and explicit forms of the tensors of elasticity for strongly anisotropic continuum fiber-reinforced composites at finite strain. *International Journal of Solids and Structures* 2002; **39**(8):2343–2358.
6. Limbert G, Taylor M, Middleton J. Three-dimensional finite element modelling of the human acl: simulation of passive knee flexion with a stressed and stress-free acl. *Journal of Biomechanics* 2004; **37**(11):1723–1731.
7. Ehret AE, Itskov M. Modeling of anisotropic softening phenomena: Application to soft biological tissues. *International Journal of Plasticity* 2009; **25**(5):901–919.
8. Giles JM, Black AE, Bischoff JE. Anomalous rate dependence of the preconditioned response of soft tissue during load controlled deformation. *Journal of Biomechanics* 2007; **40**(4):777–785.
9. Shergold OA, Fleck NA, Radford D. The uniaxial stress versus strain response of pig skin and silicone rubber at low and high strain rates. *International Journal of Impact Engineering* 2006; **32**(9):1384–1402.

10. Muñoz MJ, Bea JA, Rodríguez JF, Ochoa I, Grasa J, Pérez Del Palomar A, Zaragoza P, Osta R, Doblaré M. An experimental study of the mouse skin behaviour: Damage and inelastic aspects. *Journal of Biomechanics* 2008; **41**(1):93–99.
11. Daly CH, Odland GF. Age-related changes in the mechanical properties of human skin. *The Journal of Investigative Dermatology* 1979; **73**(1):84–87.
12. Fancello EA, Ponthot JP, Stainier L. A variational formulation of constitutive models and updates in nonlinear finite viscoelasticity. *International Journal for Numerical Methods in Engineering* 2006; **65**(11):1831–1864.
13. Ortiz M, Stainier L. The variational formulation of viscoplastic constitutive updates. *Computer Methods in Applied Mechanics and Engineering* 1999; **171**(3–4):419–444.
14. Radovitzky R, Ortiz M. Error estimation and adaptive meshing in strongly nonlinear dynamic problems. *Computer Methods in Applied Mechanics and Engineering* 1999; **172**(1–4):203–240.
15. Weinberg K, Mota A, Ortiz M. A variational constitutive model for porous metal plasticity. *Computational Mechanics* 2006; **37**(2):142–152.
16. Ortiz M, Pandolfi A. A variational Cam-clay theory of plasticity. *Computer Methods in Applied Mechanics and Engineering* 2004; **193**(27–29):2645–2666.
17. Fancello EA, Vigneron L, Ponthot JP, Stainier L. A Viscoelastic Formulation for Finite Strains: Application to Brain Soft Tissue. *Proceedings of XXVII CILAMCE – Iberian Latin American Congress on Computational Methods in Engineering*, vol. 1, Belém, Brazil, 2006.
18. El Sayed T, Mota A, Fraternali F, Ortiz M. A variational constitutive model for soft biological tissues. *Journal of Biomechanics* 2008; **41**(7):1458–1466.
19. El Sayed T, Mota A, Fraternali F, Ortiz M. Biomechanics of traumatic brain injury. *Computer Methods in Applied Mechanics and Engineering* 2008; **197**(51–52):4692–4701.
20. Fancello EA, Vassoler JM, Stainier L. A variational constitutive update algorithm for a set of isotropic hyperelastic viscoplastic material models. *Computer Methods in Applied Mechanics and Engineering* 2008; **197**(49–50):4132–4148.
21. Holzapfel GA. *Nonlinear Solid Mechanics: A Continuum Approach for Engineering*. John Wiley & Sons: Chichester, UK, 2000.
22. Anand L, Weber G. Finite deformations constitutive equations and a time integration procedure for isotropic hyperelastic-viscoplastic solids. *Computer Methods in Applied Mechanics and Engineering* 1990; **79**(2):173–202.
23. Eaton JW. *GNU Octave Manual*, Network Theory Limited, 2002.
24. METAFOR. *Software for Thermo-Mechanical Analysis of Structures in Large Strain Regime, Mécanique Numérique Non Linéaire*. Département Aérospatiale & Mécanique, Université de Liège: Belgium.